Integrated Flight/Propulsion Control System Design Based on a Centralized Approach

Sanjay Garg* and Duane L. Mattern†
Sverdrup Technology, Inc., Cleveland, Ohio 44135
and
Randy E. Bullard‡
NASA Lewis Research Center, Cleveland, Ohio 44135

In this paper an integrated flight/propulsion control system design is presented for the piloted longitudinal landing task with a modern, statically unstable, fighter aircraft. A centralized compensator based on the linear quadratic Gaussian/loop transfer recovery methodology is first obtained to satisfy the feedback loop performance and robustness specifications. This high-order centralized compensator is then partitioned into airframe and engine "subcontrollers" based on modal controllability/observability for the compensator modes, and the subcontrollers are further reduced in order and simplified. These subcontrollers have the advantage that they can be implemented as separate controllers on the airframe and the engine while still retaining the important performance and stability characteristics of the full-order centralized compensator. Command prefilters are then designed for the closed-loop system, and the overall system performance evaluation results are presented.

Nomenclature

$E[\ ]$	= expected value of [ ]
$G(s)$	= plant transfer function matrix
I	= identity matrix
$K(s)$	= compensator transfer function matrix
K_F, K_C	= filter and regulator gains, respectively
S_u, S_y	= diagonal matrices for scaling plant inputs and outputs
$T(s)$	= closed-loop transmission transfer matrix
p, ρ, v	= parameters used in linear quadratic Gaussian/loop transfer recovery
e	= error (commanded − actual)
s	= Laplace variable
Γ	= process noise distribution matrix, subcontroller interface matrix
μ	= stability robustness measure
σ_i	= ith singular value
$\underline{\sigma}, \bar{\sigma}$	= minimum and maximum singular value
ω	= frequency, rad/s

Subscripts

a	= airframe system
ae	= interface from engine (propulsion) system to airframe subcontroller
c	= commanded value, compensator
e	= propulsion system
ea	= interface from airframe system to engine subcontroller
p	= plant
p_s	= scaled plant
s	= scaled value

Received July 20, 1989; presented as Paper 89-3520 at the AIAA Guidance, Navigation, and Control Conference, Boston, MA, Aug. 14-16, 1989; revision received Dec. 13, 1989.

*Controls Engineer, Lewis Research Center Group. Senior Member AIAA.
†Controls Engineer, Lewis Research Center Group.
‡Control Systems Engineer, currently with M. K. Ferguson Co., Cleveland, OH.

Introduction

THE desire to enlarge the flight envelope of tactical aircraft and provide new/enhanced maneuver capabilities has led to the use of forces and moments produced by the propulsion system to augment the flight control function. The coupling between the propulsion system dynamics and the airframe dynamics, which results from such an application of the propulsion system forces and moments, is significant enough that the traditional approach of designing the propulsion control system and the flight control system separately and then putting them together in an ad hoc manner may no longer be adequate. An integrated approach to flight/propulsion control system design is then required in order to obtain an overall system that will ensure optimum performance with minimum pilot workload.

Two very different approaches to integrated flight/propulsion control design that have appeared in the recent literature include the following:

1) A linear quadratic Gaussian/loop transfer recovery- (LQG/LTR-) based centralized approach that consists of designing a "global" integrated compensator considering the fully integrated system as one high-order system.[1]

2) A decentralized, hierarchical approach that consists of partitioning the integrated system into loosely coupled subsystems and then designing separate controllers for the subsystems, using linear quadratic regulator- (LQR-) based explicit model-following type of approach, such that some high-level performance criteria are met.[2]

The objectives of this study were to gain extensive insight into the centralized integrated control design approach (approach 1) and evaluate the strengths and weaknesses of the methodology with regard to its application to integrated flight/propulsion control design for short takeoff and vertical landing (STOVL) aircraft envisaged for the future.[3] Toward these goals, results are reported in this paper from an example application of this LQG/LTR-based methodology to integrated flight/propulsion control design for the piloted longitudinal landing task with a modern, statically unstable flighter aircraft. However, this study takes the integrated control design process a step beyond that reported in Ref. 1 in that the high-order centralized compensator is partitioned into simplified lower-order subcontrollers that can be implemented

separately on the airframe and the engine without any significant loss of overall system performance and robustness.

In the following, the LQR/LTR-based integrated control law design procedure is first briefly summarized. The vehicle model is then discussed, and the design specifications are stated. The centralized feedback compensator design is then presented, and the closed-loop performance and robustness characteristics are discussed. The procedure for partitioning the centralized compensator into separate airframe and engine subcontrollers is discussed next, and closed-loop evaluation results are presented for the system consisting of the simplified subcontrollers. Finally, prefilter design results are presented to provide command shaping such that the closed-loop system response to airframe and engine command inputs is as desired.

Control Law Design Methodology

The salient features of the LQG/LTR-based control design methodology are briefly discussed in the following. This discussion is based on the description of the methodology in Ref. 4.

The nonlinear simulation of the complete aircraft system is first used to obtain linear models at various design points along the aircraft flight envelope. An open-loop analysis of the plant, at each design point, is performed to assess the number of degrees of freedom and to define the candidate variables to be regulated and/or commanded. Further dynamics such as integrators, are also appended to the plant to provide desirable feedback-loop properties.

The control design structure consists of feedback control with command shaping, as shown in the block diagram of Fig. 1. Design goals are used to generate requirements on feedback-loop properties and on command shaping prefilters. The feedback compensator $K(s)$ is designed first using a LQG with LTR approach.[5,6] After the feedback design is complete, the command shaping $P(s)$ is designed with a multivariable band-limited inverse method.[7] This method consists of formulating the prefilter design problem as a separate regulator problem and provides for setting the bandwidth of the prefiltering action by properly selecting the control weighting in the regulator problem. Such an approach allows the designer to obtain a prefilter $P(s)$ for desired response to command inputs without altering the feedback properties.

The command shaping and feedback compensator designs can be performed for the various design points covering the aircraft flight envelope, and a practical controller for the full flight envelope can be obtained by gain scheduling the designs, adding limiting functions, etc. In this study, however, the control design will be performed for only one fixed point along the approach and landing trajectory.

A major criticism of a centralized integrated control design approach, such as the one just discussed, is that it results in *one* high-order complicated compensator that is very difficult to implement. Such a compensator might also result in many feedback paths that are not physically realizable. Also, traditionally it is the responsibility of the engine designer/manufacturer to ensure that the engine will provide the desired performance when installed in the airframe. The engine manufacturer performs extensive "bench tests" with an active engine controller to ensure an adequate design. The accountability issue, then, becomes a major political hurdle with a centralized airframe and engine compensator. To address these difficulties, the idea of partitioning the centralized compensator into separate airframe and engine subcontrollers, without any significant loss in overall system performance, is introduced in this paper.

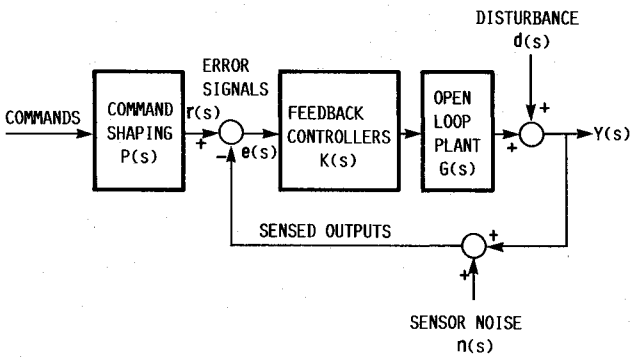

Fig. 1 Block diagram of feedback control with command shaping.

Vehicle Model

The vehicle model consists of an integrated airframe and propulsion system state space representation for a modern fighter aircraft powered by a two-spool turbofan engine and equipped with a two-dimensional thrust vectoring and reversing nozzle. The vehicle dynamics are linearized at an airspeed $V_0 = 120$ kts and flight-path angle $\gamma_0 = -3$ deg. This flight condition is representative of the short takeoff and landing (STOL) approach-to-landing task. The vehicle model has the form

$$\dot{\bar{x}}_p = A_p\bar{x}_p + B_p\bar{u}_p; \qquad \bar{y}_p = C_p\bar{x}_p + D_p\bar{u}_p \tag{1}$$

where the state vector is

$$\bar{x}_p = [u, w, q, \theta, h, N2, N25, P6, T41B]^T$$

with

u	= aircraft body axis forward velocity, ft/s
w	= aircraft body axis vertical velocity, ft/s
q	= aircraft pitch rate, rad/s
θ	= pitch angle, rad
h	= altitude, ft
$N2$	= engine fan speed, rpm
$N25$	= core compressor speed, rpm
$P6$	= engine mixing plane pressure, psia
$T41B$	= engine high-pressure turbine blade temperature, °R

and the control input vector is

$$\bar{u}_p = [\delta_{FL}, \delta_{FT}, WF, A78, A8, \delta_{TV}]^T$$

with

δ_{FL}	= leading-edge flap deflection angle, deg
δ_{FT}	= trailing-edge flap deflection angle, deg
WF	= engine main burner fuel flow rate, lb/h
$A78$	= thrust reverser port area, in.^{2}
$A8$	= main nozzle throat area, in.^{2}
δ_{TV}	= nozzle thrust vectoring angle, deg

The vector $\bar{y}_p$ represents the outputs to be controlled and will be discussed later. The vehicle system matrix A_p and the control effectiveness matrix B_p are listed in the Appendix.

The open-loop vehicle eigenvalues are

$$\lambda_1 = 0.07, \qquad \lambda_{2,3} = -0.09 \pm j0.23,$$

$$\lambda_4 = 1.06, \qquad \lambda_5 = -1.47 \text{ (airframe modes)}$$

$$\lambda_6 = -1.40, \qquad \lambda_7 = -3.57,$$

$$\lambda_8 = -6.96, \qquad \lambda_9 = -89.28 \text{ (propulsion modes)}$$

Note that the airframe is statically unstable with a highly unstable pitch mode. Analysis of the control distribution matrix B_p indicated that the flaps δ_{FL} and δ_{FT} and thrust vectoring δ_{TV} are primarily airframe controls with very little effect on the propulsion system dynamics, whereas the fuel

flow WF and the area controls $A78$ and $A8$ affect both the airframe and the engine dynamics. Thrust vectoring δ_{TV} is the primary pitch control, whereas the flaps are direct-lift devices that provide direct control of the flight-path angle.

For the STOL approach and landing task, it is desirable to provide the pilot with decoupled control of flight path and airspeed. Open-loop analyses of the plant indicated that the available flap control authority and the resulting flight-path control effectiveness were not adequate enough to provide flight-path control independent of the pitch attitude control. Therefore, the control law design objective was chosen as that of providing independent control of pitch attitude and airspeed from pilot inputs with the flaps used to augment the aircraft flight-path to pitch attitude (γ/θ) response. The desired γ/θ response for the STOL task is

$$\frac{\gamma}{\theta}(s)\bigg|_{\text{desired}} \approx \frac{1/\tau_{\theta_2}}{s + 1/\tau_{\theta_2}}$$

where (s) represents the Laplace operator. The level I handling qualities requirements[8] are that $1/\tau_{\theta_2} \geq 0.7\ \text{s}^{-1}$. From the numerator of the open-loop pitch attitude response to δ_{TV} input, the value of $1/\tau_{\theta_2}$ was found to be $0.27\ \text{s}^{-1}$, indicating that flight-path augmentation will be necessary to obtain an acceptable system. It was not at all clear as to how the LQG/LTR-based integrated control design methodology could be used to formulate the problem in such a manner as to directly synthesize the desired flight-path to pitch attitude response. Therefore, prior to applying the control design methodology, classical single-input/single-output control law design techniques were used to augment the flight-path response. Since the flaps are direct-lift devices, a constant-gain loop closure from angle of attack to the flaps, i.e., $\delta_{FL} = -K_1\alpha$ and $\delta_{FT} = -K_2\alpha$ with $\alpha = C_\alpha \bar{x}_p$, will effectively increase the value of $1/\tau_{\theta_2}$. The numerical value of the matrix C_α is listed in the Appendix. Based on open-loop evaluation of the effectiveness of the flaps, the gains K_1 and K_2 were chosen so that $K_2 = -K_1$. Based on the theory of coupling numerators,[9] the root-locus technique was used to study the effect of these loop closures on the zeros of the numerator of $(\theta/\delta_{TV})(s)$ transfer function. A detailed example of this procedure can be found in Ref. 10. A value of $K_1 = 3$ deg/deg resulted in $1/\tau_{\theta_2} = 0.52\ \text{s}^{-1}$. Although $1/\tau_{\theta_2}$ could be increased further by increasing K_1, doing so will result in excessive flap deflections. Therefore, $K_1 = 3$ deg/deg was used as a reasonable compromise between handling quality requirements and flap deflection constraints. With the flap loops closed, the control inputs available for the feedback compensator design are

$$\bar{u}'_p = [WF, A78, A8, \delta_{TV}]^T$$

For the rest of this paper, the vehicle model with the flap loops closed as described earlier will be considered to be the design model.

Feedback Compensator Design and Evaluation

The following design specifications for the feedback compensator were chosen: 1) track airframe and engine commands in a decoupled manner and with zero steady-state error for step commands; 2) maintain "adequate" stability margins in all control loops to guarantee stability in the presence of unmodeled dynamics and variation in model parameters; and 3) avoid "excessive" control deflections and rates to prevent nonlinearities due to control deflection and/or rate limiting.

As stated earlier, the control design objective is to provide the pilot with independent control of aircraft airspeed and pitch attitude. In the STOL mode, thrust reversing is used to allow higher-frequency control of the forward velocity. To effectively use thrust reversing, the engine is maintained at military power level. This power setting will use the engine fan speed and engine pressure ratio set points from the baseline engine control schedule. Thus, the airframe and engine outputs to be controlled are

$$\bar{y}_p = [V, q_v, N2P, \text{EPR}]^T$$

where

V = aircraft airspeed (ft/s)
q_v = pitch variable $= q + 0.1\theta$
$N2P$ = engine fan speed (% of maximum allowable rpm at operating condition)
EPR = engine pressure ratio

The C_p matrix corresponding to these outputs is listed in the Appendix, and the D_p matrix is $\bar{0}$. Note that the choice of q_v reflects the desire to track pitch rate commands at high frequencies and pitch attitude commands at low frequencies. This choice is consistent with the work reported in Ref. 4.

Based on performance requirements, stability robustness to unmodeled dynamics such as actuators and sensors, and the open-loop analyses of control effectiveness, the desired control bandwidths were chosen as 1 rad/s for the V loop, 5 rad/s for the q_v loop, 5 rad/s for the $N2$ loop, and 10 rad/s for the EPR loop.

As pointed out in Ref. 11, it is very important to properly scale the system of Eq. (1) prior to applying the LQG/LTR methodology in order for the methodology to lead to the desired results. For the present study, an input/output scaling of the following form was used:

$$\bar{u}_{p_s} = S_u \bar{u}'_p; \qquad \bar{y}_{p_s} = S_y \bar{y}_p$$

resulting in a scaled system of the form

$$\dot{\bar{x}}_p = A'_p \bar{x}_p + B_{p_s} \bar{u}_{p_s}; \qquad \bar{y}_{p_s} = C_{p_s} \bar{x}_p \tag{2}$$

where $B_{p_s} = B'_p S_u^{-1}$ and $C_{p_s} = S_y C_p$. Here, B'_p is the control distribution matrix corresponding to the control inputs $\bar{u}'_p$, and A'_p is the plant matrix with the flap loops closed. The numerical values of S_u and S_y, listed in the Appendix, correspond to normalizing the control inputs by their maximum allowable variations from trim and the controlled outputs by the maximum values to be commanded.

Since the vehicle model has no integrators, and a zero steady-state error for step commands is desired, integral control action (see Ref. 12) is provided by appending four integrators to the plant—one in each control channel. The augmented plant has the form

$$\dot{\bar{x}} = A\bar{x} + B\bar{u}; \qquad \bar{y} = C\bar{x} \tag{3}$$

where $\bar{x} = [\bar{x}_p^T, \bar{u}_{p_s}^T]^T$ with $\bar{x}_p$ and $\bar{u}_{p_s}$ as defined earlier, and $\bar{y} = \bar{y}_{p_s}$. The system matrices A, B, and C for the scaled, augmented plant are given by

$$A = \begin{bmatrix} A'_p & B_{p_s} \\ 0 & 0 \end{bmatrix}; \qquad B = \begin{bmatrix} 0 \\ I \end{bmatrix}; \qquad C = [C_{p_s} 0] \tag{4}$$

where I is an appropriately dimensioned identity matrix.

The LQG/LTR procedure is based on solving for the optimal compensator that minimizes the performance index,

$$J_p = E\left\{ \lim_{T\to\infty} \frac{1}{T} \int_0^T [(\bar{z}^T\bar{z} + p\bar{y}^T V \bar{y}) + \rho \bar{u}^T \bar{u}]\, dt \right\} \tag{5}$$

for a system of the form

$$\dot{\bar{x}} = Ax + B\bar{u} + \Gamma\bar{\xi}; \qquad \bar{y} = C\bar{x} + v I\bar{\eta}; \qquad \bar{z} = H\bar{x} \tag{6}$$

where $\bar{\xi}$ and $\bar{\eta}$ are zero-mean Gaussian white-noise processes

with identity intensity, $\bar{y}$ are the measurements available as compensator inputs, and $\bar{z}$ are the controlled plant outputs. V is any positive-definite symmetrical weighting matrix, and v, p, ρ, and the process noise distribution matrix Γ are the design parameters that are used in the LQG/LTR procedure to synthesize a compensator that would meet the desired specifications. The procedure consists of first designing the Kalman filter so that the filter loop satisfies the performance and stability robustness requirements and then recovering this loop asymptotically by tuning the regulator. The Kalman filter gains K_F and the regulator gains K_C are obtained by solving their respective algebraic Riccati equations.[12] Note here that the numerical value of J_p and the Γ have no physical significance. The Kalman filter is not actually being designed for state estimation; rather, the formulation in Eq. (5) is used strictly to exploit the known properties of the quadratic optimal control solution. The LQG/LTR compensator has the following form:

$$K_{\mathrm{LQG/LTR}}(s) = K_C[sI - (A - BK_C - K_FC)]^{-1}K_F \qquad (7)$$

A detailed discussion of how to choose the LQG/LTR design parameters is available in various application studies of the LQG/LTR methodology (see, for example, Refs. 13 and 14). For instance, it is shown that if the Kalman filter loop is to meet the design specifications, then Γ and v should be selected in such a way that the target feedback loop transfer function matrix $G_{FOL}(s)$, defined as

$$G_{FOL}(s) = (1/\sqrt{v})C(sI - A)^{-1}\Gamma$$

has the desired loop shapes. From the design specifications stated earlier, the requirement on $G_{FOL}(s)$ is

$$G_{FOL}(S) \cong \frac{1}{s} \cdot \mathrm{diag}[1, 5, 5, 10]$$

i.e., bandwidth of 1, 5, 5, and 10 rad/s for the V, q_v, $N2$, and EPR loops, respectively; k/s behavior at loop crossover for stability robustness; and large low-frequency gains for accurate steady-state tracking of commands.

For the integrated control problem considered here, the controlled variables are the same as the measurements, i.e., $H = C$, and the matrices A, B, and C are as defined in Eq. (4). A study of the singular values of the scaled, augmented plant ($\sigma_i[G(j\omega)]$, where $G(s) = C(sI - A)^{-1}B$), indicated that the design plant $G(s)$ has the desired loop shapes; thus, the choice $\Gamma = B$ can be used to define the target feedback loop $[G_{FOL}(s)]$ in the synthesis of the filter gains K_F.

The block diagram for the LQG/LTR compensator design is shown in Fig. 2. In Fig. 2 $G_p(s)$ is the transfer function matrix of the vehicle model with the flap loops closed. With $\rho = 1$ and $V = I$ in Eq. (5), an LQG/LTR compensator that satisfies the desired command tracking bandwidth requirements was obtained for the design parameter values $v = 0.64$ and $p = 10^4$. Note that although choosing a higher value of p would have lead to a better recovery of the Kalman filter loop and the associated guaranteed stability margins, doing so would also have resulted in larger control bandwidth requirements. The singular values of the loop transfer matrix at the plant output ($\sigma_i[GK(j\omega)]$ with $K(j\omega) = K_{\mathrm{LQG/LTR}}(j\omega)$) are shown in Fig. 3. In Fig. 3 the large loop gains at low frequencies indicate the desirable properties of good command tracking and disturbance rejection, and the loop bandwidths are from 1 to 10 rad/s, providing adequate roll-off at higher frequencies to maintain stability in the presence of unmodeled dynamics.

The closed-loop system tracking performance was evaluated by studying the Bode plots of the closed-loop system frequency response to commanded inputs and time histories of closed-loop response to step commanded inputs. The frequency response of velocity V to all the commanded inputs (V_c, q_{v_c}, $N2P_c$, and EPR_c) is shown in Fig. 4 as an example

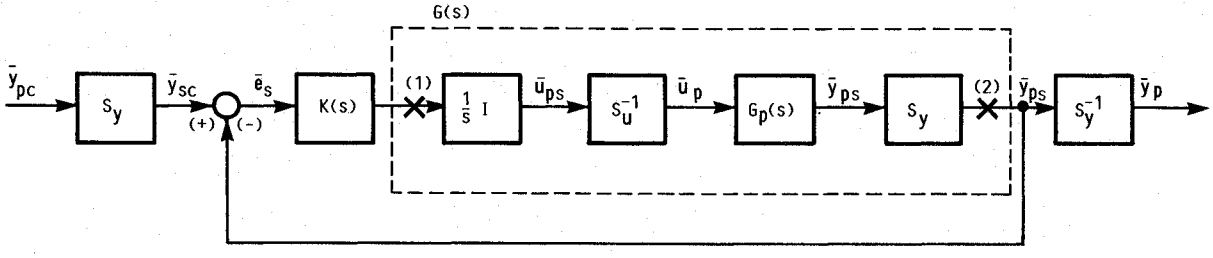

Fig. 2 Block diagram for LQG/LTR compensator design.

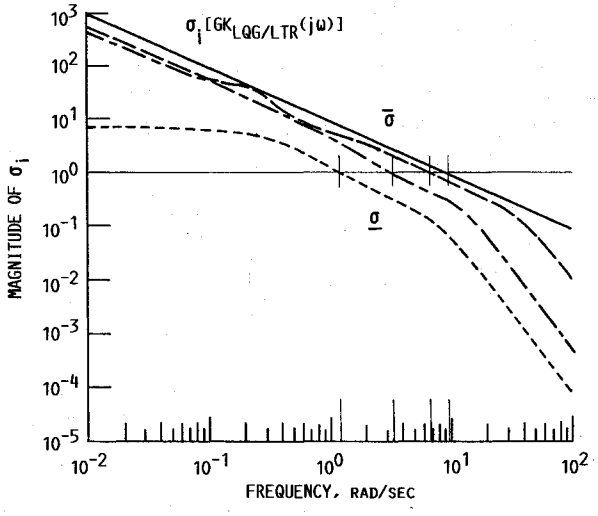

Fig. 3 Loop transfer matrix singular values with LQG/LTR compensator, $\sigma_i[GK_{\mathrm{LQG/LTR}}(j\omega)]$.

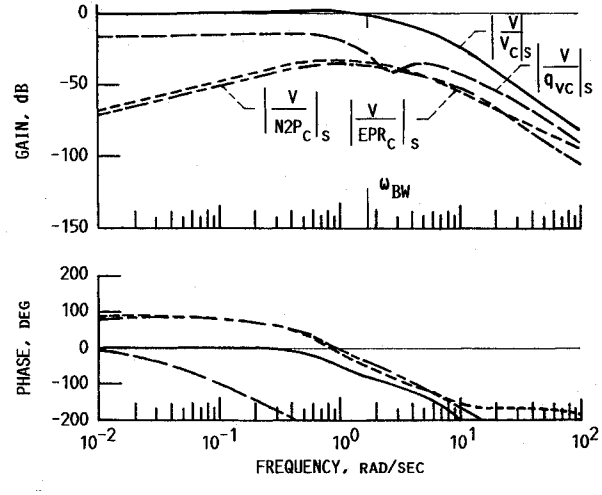

Fig. 4 Closed-loop Bode plots of aircraft velocity V, response to command inputs (V_c, q_{v_c}, $N2P_c$, and EPR_c): scaled system.

of the Bode plots that were studied. Note that the quantities shown in Fig. 4 are scaled quantities (corresponding to $\bar{y}_{ps}$ and $\bar{y}_{sc}$ of Fig. 2), so that the response magnitudes can be compared one-to-one to assess the degree of coupling/decoupling in the closed-loop system response. As seen from Fig. 4, the feedback compensator provides accurate tracking of velocity commands up to the desired bandwidth with insignificant response in velocity to other commanded variables. The bandwidths of the q_v, $N2$, and EPR loops were also close to the design specifications. The time-domain analysis of closed-loop system response to step commands also showed decoupled command tracking with well-damped response and fast rise times for the q_v, $N2$, and EPR responses. Note that, apart from good command tracking performance, it is also important to make sure that the feedback compensator does not result in excessive variations in other variables such as compressor and turbine stall margins and high-pressure turbine blade temperature, which are of interest from the point of safe operation of the engine. The responses of these variables were studied for the present compensator design and were found to be within allowable limits for maximum step commands in the controlled variables.

Extensive stability robustness studies, using the singular value approach,[15,16] were performed for this feedback compensator design. Although a realistic robustness test of the compensator will require nonlinear simulation evaluation over the design portion of the flight envelope, the current study focused on analyzing robustness to linear perturbations because of the nonavailability of a complete nonlinear simulation. The effect on closed-loop system stability due to including some representative actuator and sensor dynamics was first studied. The details of this study are available in Ref. 17. It was found that the singular value condition that guarantees the stability of the closed-loop system, treating the actuator and sensor dynamics as modeling errors, was violated. However, eigenvalue analysis with these same actuator and sensor dynamics showed the closed-loop system to be stable. This result points to the conservativeness of the singular value analysis approach and to the need to develop improved procedures for stability robustness analysis of multivariable systems.

Lehtomaki et al.[16] have shown that, for multi-input/multi-output systems, the minimum singular value of the return difference matrix, calculated at the plant output or input, is a reliable measure of closed-loop system stability robustness to unstructured uncertainties occurring at the plant input or output. For the present feedback compensator design, the lowest value of the minimum singular value of the return difference matrix at the design plant output ($\underline{\sigma}[I + GK(j\omega)]$) was 0.72 and that at the design plant input ($\underline{\sigma}[I + KG(j\omega)]$) was 0.65. These values indicate reasonable stability robustness to unstructured uncertainties. However, it is important to realize that these stability robustness properties are guaranteed for the loops broken at points 1 and 2 in the LQG/LTR compensator design block diagram of Fig. 2. The actual control system implementation will be as shown in the block diagram of Fig. 5, wherein the interface between the physical system [$G_p(s) = C_p(sI - A_p')^{-1}B_p'$ for the present case] and the control system [$K_p(s)$] is at points 1′ and 2′. It is at these points in the loop that we need "good" stability margins. The lowest values of the minimum singular value of the return difference matrix at points 1′ and 2′, minimum over ω of $\underline{\sigma}[I + K_pG_p(j\omega)]$ and $\underline{\sigma}[I + G_pK_p]$, respectively, were found to be 0.02 and 0.1, respectively. These values indicate very poor stability robustness to unstructured uncertainties for the system as implemented in Fig. 5. From this analysis it would appear that the claim that the LQG/LTR methodology recovers the guaranteed stability robustness properties of the LQR problem is misleading. The stability robustness properties are *recovered*, but *not* at the physical interface between the plant and the control system where the effect of the modeling uncertainties will actually occur.

In control system design classical measures of stability robustness are the gain and phase margins.[18] Although the preceding results indicate that the implementation system (as in Fig. 5) will have much reduced stability robustness with respect to unstructured uncertainties compared to the design system (as in Fig. 2), it has been shown in Ref. 11 that, as far as structured uncertainty in the form of loop gain or phase variations is concerned, the implementation system will have the same guaranteed multivariable stability margins as those obtained for the design system. This result is based on a nonconservative measure of stability robustness for structured uncertainties, called μ, or the structured singular value, which has recently been developed.[19,20] The maximum overall frequencies ω of the structured singular value for gain and phase variations at points 1′, $\mu[(I + K_pG_p)^{-1}]$, and 2′, $\mu[(I + G_pK_p)^{-1}]$ were found to be 1.38 and 1.37, respectively. Using the results of Ref. 20, these maximum values of μ indicate that the closed-loop system will have guaranteed multivariable gain margins of -4.7 to 11.1 dB and phase margins of ± 42.4 deg for *simultaneous* loop gain or phase variations at the plant input or the output.

The stability robustness of the closed-loop system as implemented in Fig. 5 was further evaluated using the more classical approach of "breaking" one loop at a time (i.e., one loop open and the other loops closed). The one-loop-at-a-time analysis showed that the closed-loop system will remain stable for a gain increase of up to 15 dB or additional phase lag up to 50 deg occurring in any individual loop either at the plant input or the output. These are excellent stability margins and meet the military specifications for the operation of flight vehicles.

The control bandwidth requirements for the closed-loop system were also studied using the one-loop-at-a-time analysis. The control bandwidths for the *WF*, *A*78, *A*8, and δ_{TV} loops were found to be very much within the actuator bandwidths for the representative actuators considered earlier in the stability robustness study. The control deflection and rate requirements for tracking maximum commanded values of the controlled variables, obtained from time histories of the control input ($\bar{u}_p'$) responses to step commands ($\bar{y}_{pc}$), were also found to be reasonable and within the maximum allowable control deflections and rates.

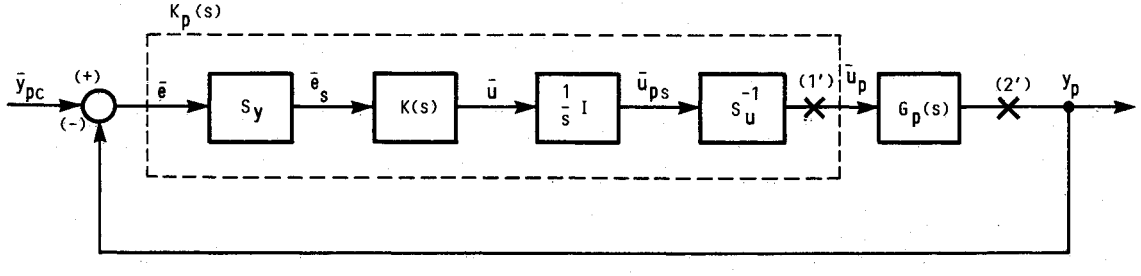

Fig. 5 Block diagram for compensator implementation.

Compensator Partitioning and Simplification

The need to separately implement controllers for the airframe and the engine was pointed out in an earlier section. In this section, the mathematical approach to partitioning the high-order integrated compensator into separate subsystem controllers is presented along with the numerical results for partitioning the LQG/LTR compensator obtained in the previous section. The partitioned subcontrollers are further reduced in state dimension and simplified for ease of implementation. Some example results are then presented to compare the closed-loop system performance and robustness for these simplified subcontrollers with those for the full-order LQG/LTR compensator. Note that partitioning the integrated compensator and then reducing the order of the subcontrollers is intuitively more meaningful than reducing the order of the integrated compensator before partitioning. In the latter case any decoupling inherent in the compensator due to the decoupled behavior of the integrated system (plant) might be lost in the process of reducing the order of the compensator, thus making the partitioning task more difficult.

Compensator Partitioning

The mathematical approach to partitioning the integrated compensator into separate (state-decoupled) subcontrollers, presented in the following, was motivated by the discussion in Ref. 2 on partitioning the integrated system (plant) into state-decoupled subsystems in order to perform the decentralized, hierarchical control system design. For ease of discussion and relevance to the present design study, the procedure is presented for partitioning into just two subcontrollers: those for the airframe and the engine. However, the procedure is clearly applicable for the more general case of more than two subcontrollers. The direct feedthrough term D_c for the compensator has also been neglected in the following to keep the equations simple. The extension to the case of the nonzero D_c matrix is quite straightforward.

Given an integrated compensator of the form

$$\dot{\bar{x}}_c = A_c\bar{x}_c + B_c\bar{e}_y; \qquad \bar{u} = C_c\bar{x}_c \tag{8}$$

we want to obtain state-decoupled subcontrollers of the following form:

Airframe controller

$$\dot{\bar{x}}_{c_a} = A_{c_a}\bar{x}_{c_a} + B_{c_a}\bar{e}_{y_a} + \Gamma_{ae}\bar{e}_{y_e}; \quad \bar{u}_a = C_{c_a}\bar{x}_{c_a} + W_{ae}\bar{u}_e \tag{9}$$

Engine controller

$$\dot{\bar{x}}_{c_e} = A_{c_e}\bar{x}_{c_e} + B_{c_e}\bar{e}_{y_e} + \Gamma_{ea}\bar{e}_{y_a}; \quad \bar{u}_e = C_{c_e}\bar{x}_{c_e} + W_{ea}\bar{u}_a \tag{10}$$

with $\bar{u}^T = [\bar{u}_a^T, \bar{u}_e^T]$ and $\bar{e}_y^T = [\bar{e}_{y_a}^T, \bar{e}_{y_e}^T]$, such that the input/output behavior ($\bar{u}$ to $\bar{e}_y$ response) of the integrated compensator is matched as best as possible. This desired partitioning is shown in the simplified block diagrams of Fig. 6. Note that, with such a partitioning, the states of one subcontroller do not directly affect the outputs of the other subcontroller. Therefore, the subcontrollers can be built as separate "black boxes" and integrated in the final implementation with the least number of interconnections. The division of the integrated compensator inputs ($\bar{e}_y$) and outputs ($\bar{u}$) into the respective subcontroller inputs ($\bar{e}_{y_a}$ and $\bar{e}_{y_e}$) and outputs ($\bar{u}_a$ and $\bar{u}_e$) is determined based on the results of the open-loop effectiveness analysis, conducted at the initialization of the control design study. This is coupled with an intimate knowledge of the physical system being controlled; i.e., the control inputs $\bar{u}_a$ into the integrated plant $[G(s)]$ are primarily effective in regulating the errors $\bar{e}_{y_a}$ with secondary response in the errors $\bar{e}_{y_e}$, and similarly for $\bar{u}_e$.

The state definition of the integrated compensator has no particular significance in terms of physical interpretation. Therefore, without loss of generality, Eq. (8) can be assumed to be in the modal form so that the matrix A_c is block diagonal. The matrices B_c and C_c are then measures of the modal controllability and observability, respectively, for the compensator modes. The modal compensator states $\bar{x}_c$ are assigned to $\bar{x}_a$ or $\bar{x}_e$ based on whether they are more controllable by $\bar{e}_{y_a}$ or $\bar{e}_{y_e}$ and/or more observable in $\bar{u}_a$ or $\bar{u}_e$. This is accomplished by considering the columns of B_c and rows of C_c one at a time and comparing the relative magnitudes of the elements in the columns/rows. From Eqs. (8–10) note that all of the integrated compensator inputs ($\bar{e}_y$) are also inputs to the state equations of the subcontrollers. This means that the modal controllability for the integrated compensator is perfectly matched in the partitioning. Therefore, in case of a conflict in assigning the integrated compensator states to $\bar{x}_a$ or $\bar{x}_e$, such as the case where a modal state is "most" controllable by an element of e_{y_a} whereas it is "most" observable in an element of $\bar{u}_e$, the assignation should be based on observability. After the division and an appropriate reordering of the compensator modal states, the state space representation for the compensator is

$$\begin{bmatrix}\dot{\bar{x}}_{c_a}\\ \dot{\bar{x}}_{c_e}\end{bmatrix} = \begin{bmatrix}A_{c_1} & 0\\ 0 & A_{c_2}\end{bmatrix}\begin{bmatrix}\bar{x}_{c_a}\\ \bar{x}_{c_e}\end{bmatrix} + \begin{bmatrix}B_{c_{11}} & B_{c_{12}}\\ B_{c_{21}} & B_{c_{22}}\end{bmatrix}\begin{bmatrix}\bar{e}_{y_a}\\ \bar{e}_{y_e}\end{bmatrix} \tag{11a}$$

$$\begin{bmatrix}\bar{u}_a\\ \bar{u}_e\end{bmatrix} = \begin{bmatrix}C_{c_{11}} & C_{c_{12}}\\ C_{c_{21}} & C_{c_{22}}\end{bmatrix}\begin{bmatrix}\bar{x}_{c_a}\\ \bar{x}_{c_e}\end{bmatrix} \tag{11b}$$

From a direct comparison of Eqs. (9) and (10) with Eqs. (11), we get $A_{c_a} = A_{c_1}$, $B_{c_a} = B_{c_{11}}$, $\Gamma_{ae} = B_{c_{12}}$, and $A_{c_e} = A_{c_2}$, $B_{c_e} = B_{c_{22}}$ and $\Gamma_{ea} = B_{c_{21}}$, Thus, the only approximation involved in the partitioning is that of approximating the contribution of the states of one subcontroller to the outputs of the other subcontroller. Simple algebraic manipulation of Eqs. (9–11) leads to the following solution:

$$W_{ae} = C_{c_{12}}C_{c_{22}}^{\#}; \qquad C_{c_a} = C_{c_{11}} - W_{ae}C_{c_{21}} \tag{12a}$$

$$W_{ea} = C_{c_{21}}C_{c_{11}}^{\#}; \qquad C_{c_e} = C_{c_{22}} - W_{ea}C_{c_{12}} \tag{12b}$$

where $(\,)^{\#}$ denotes the pseudoinverse of $(\,)$. For numerical accuracy singular value decomposition-based procedures[21] are used to solve for the pseudoinverse.

For the LQG/LTR design compensator being considered here, from Fig. 2 the compensator inputs are the scaled tracking errors, i.e., $\bar{e}_y = [e_{V_s}, e_{q_{vs}}, e_{N2P_s}, e_{\mathrm{EPR}_s}]^T$ with $e_{V_s} \equiv V_{c_s} - V_s$, and similarly for other errors with $(\,)_s$ denoting scaled quantities. The LQG/LTR compensator outputs are the derivatives of the scaled control inputs, i.e., $\bar{u} = [WF\dot{}_s, A7\dot{8}_s, A8\dot{}_s, \dot{\delta}_{TV_s}]^T$, and the compensator is of 13th order, i.e., $\dim(\dot{\bar{x}}_c) = 13$. Earlier open-loop analyses indicated that δ_{TV} is primarily a pitch effector, whereas WF, $A78$, and $A8$ mainly affect the engine control variables ($N2$ and EPR) and the airspeed (V). Therefore, the following subcontroller input/output pairings were chosen for compensator partitioning:

$$\bar{e}_{y_a} = e_{q_{vs}}; \qquad \bar{u}_a = \dot{\delta}_{TV_s} \tag{13a}$$

$$\bar{e}_{y_e} = [e_{V_s}, e_{N2P_s}, e_{\mathrm{EPR}_s}]^T; \qquad \bar{u}_e = [WF\dot{}_s, A7\dot{8}_s, A8\dot{}_s]^T \tag{13b}$$

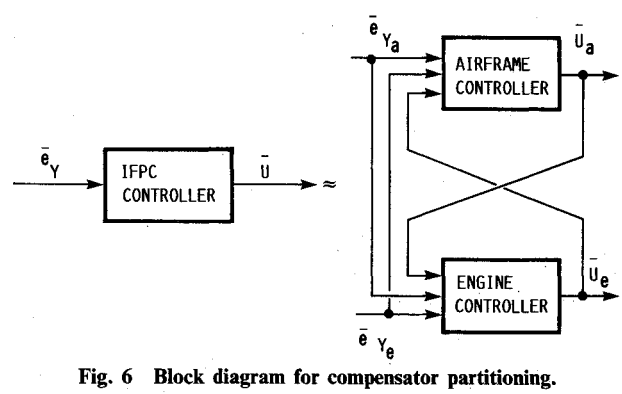

Fig. 6 Block diagram for compensator partitioning.

The compensator modal controllability/observability studies, as discussed earlier, resulted in a fifth-order airframe subcontroller [$\dim(\bar{x}_{c_a}) = 5$] and an eighth-order engine subcontroller [$\dim(\bar{x}_{c_e}) = 8$]. This compensator partitioning was validated by comparing the LQG/LTR compensator singular values ($\sigma_i[K_{\mathrm{LQG/LTR}}(j\omega)]$) with the singular values of the integrated compensator obtained by assembling the partitioned subcontrollers [i.e., combining Eqs. (9) and (10) in the form of Eqs. (8)] and the singular values of the corresponding loop transfer matrices ($\sigma_i[GK(j\omega)]$) and closed-loop response matrices ($\sigma_i[T_s(j\omega)]$, with $\bar{y}(s) = T_s(s) \cdot \bar{y}_{c_s}(s)$). Excellent matching was obtained for all these comparisons, indicating that the closed-loop performance and the desirable feedback properties of the integrated LQG/LTR compensator are retained in the partitioned subcontrollers. Example comparison results are presented after the subcontroller order reduction and simplification is discussed in the following subsection.

Subcontroller Order Reduction and Simplification

For ease of implementation it is desirable to further reduce the order of the subcontrollers and simplify the structure by eliminating the insignificant feedbacks. Each of the subcontrollers, from Eqs. (9) and (10), can be represented in the form

$$\dot{\bar{x}}_{c_i} = A_{c_i}\bar{x}_{c_i} + B'_{c_i}\bar{e}'_{y_i}; \qquad \bar{u}_i = C_{c_i}x_{c_i} + D'_{c_i}e'_{y_i} \tag{14}$$

with $e'_{y_i} \equiv \mathrm{col}[\bar{e}_{y_i}, \bar{e}_{y_j}]$ and corresponding definitions of B'_{c_i} and D'_{c_i}. The model reduction technique based on internally balanced realizations[22] can then be used on a system in the form given in Eqs. (14) to obtain reduced-order subcontrollers. Note that, in general, a frequency-weighted internally balanced reduction technique[23] has been shown to lead to a "better" lower-order approximation for controller reduction. However, in the present design study the frequency-weighted technique is quite cumbersome to apply, since the state space realization of the frequency weighting, suggested in Ref. 23, will itself be of very high order.

Using the internally balanced realization approach, the order of the airframe controller was reduced from 5 to 2 and that of the engine controller from 8 to 7. The system matrices for these reduced order subcontrollers, consistent with the definitions in Eqs. (9) and (10) and corresponding to the input/output pairings of Eqs. (13), are listed in the Appendix. From the data in the Appendix we note that there is very little direct coupling from the output of one subcontroller into the output of other subcontroller (i.e., W_{ea} and W_{ae} are ≈ 0), and also the engine control variable errors (e_{N2P_s} and e_{EPR_s}) do not significantly drive the states of the airframe subcontroller [i.e., the last two columns of Γ_{ae} ($\Gamma_{ae}(:, 2:3)$) are ≈ 0]. Therefore, the subcontrollers were simplified with $W_{ae} = 0$, $W_{ea} = 0$ and $\Gamma_{ae}(:, 2:3) = 0$. Note that the fact that such a simplification was possible in the present example indicates that the coupling between the airframe dynamics and the engine dynamics is not very strong. Such will not be the case in general for the STOVL aircraft being considered for the future.

The loop transfer matrix singular values ($\sigma_i[GK(j\omega)]$), with $K(j\omega)$ corresponding to the compensator obtained by assembling the reduced-order and simplified subcontrollers, were found to be quite close to those corresponding to the loop shapes obtained with the LQG/LTR compensator (shown in Fig. 3), showing that the loop shapes are preserved in the compensator partitioning and simplification. The closed-loop response singular values ($\sigma_i[T_s(j\omega)]$) with the LQG/LTR compensator and with the assembled, simplified subcontrollers are compared in Fig. 7. Note that only the maximum and minimum singular values are shown in Fig. 7 to avoid cluttering the figure. The plots in Fig. 7 show that there will be no noticable change in closed-loop system performance on partitioning and simplifying the compensators.

The closed-loop system block diagram with the simplified subcontrollers is shown in Fig. 8. The representation in Fig. 8 is consistent with that in Fig. 5; i.e. the integrators appended to the plant for compensator design and the input/output scaling matrices are incorporated in the airframe and engine subcontrollers. The blocks marked $P_{(\,)}$ in Fig. 8 correspond to the command shaping filters and are discussed in the following section. Also, as shown in Fig. 8, the engine control variable commands ($N2P_{\mathrm{sel}}$ and $\mathrm{EPR}_{\mathrm{sel}}$) will be generated by the engine scheduling control system. The discussion of the engine scheduling is beyond the scope of the research reported herein, since it requires knowledge of the nonlinear behavior of the propulsion system dynamics.

Prefilter Design

With a satisfactory feedback compensator obtained as described earlier, the next step in the integrated control design procedure is to design command shaping prefilters to obtain the desired response to airframe and engine command inputs. As shown in Fig. 8, separate single-input/single-output prefilters were designed for each controlled variable as decoupled responses to pilot and engine command inputs [δ_{st} (in.) and V_{sel}, and $N2P_{\mathrm{sel}}$ and $\mathrm{EPR}_{\mathrm{sel}}$, respectively] were desired, and the feedback compensator itself provides decoupled tracking of the commanded variables.

The desired controlled variable responses to pilot and engine command inputs are listed in Table 1 in transfer function form. In Table 1 the velocity response choice is such as to result in a well-damped response with minimal overshoot and a rapid settling time with a rise time $t_{r_{90}} = 5$ s, and the pitch rate response (q/δ_{st}) selection is based on desired short period characteristics for level I handling qualities.[8] The $N2P$ and EPR response selections are based on the desired command tracking bandwidths.

Table 1 Desired response transfer functions

Notation: $\{K(1/\tau)[\zeta; \omega_n] \equiv K(s + 1/\tau)(s^2 + 2\zeta\omega_n s + \omega_n^2)\}$

$$\frac{V}{V_{\mathrm{sel}}} = \frac{0.04(3.13)}{[0.89; 0.36]}; \qquad \frac{q}{\delta_{st}} = \frac{35.12(0.5)}{[0.89; 2.24]}$$

$$\frac{N2P}{N2P_{\mathrm{sel}}} = \frac{5.0}{(5.0)}; \qquad \frac{\mathrm{EPR}}{\mathrm{EPR}_{\mathrm{sel}}} = \frac{10.0}{(10.0)}$$

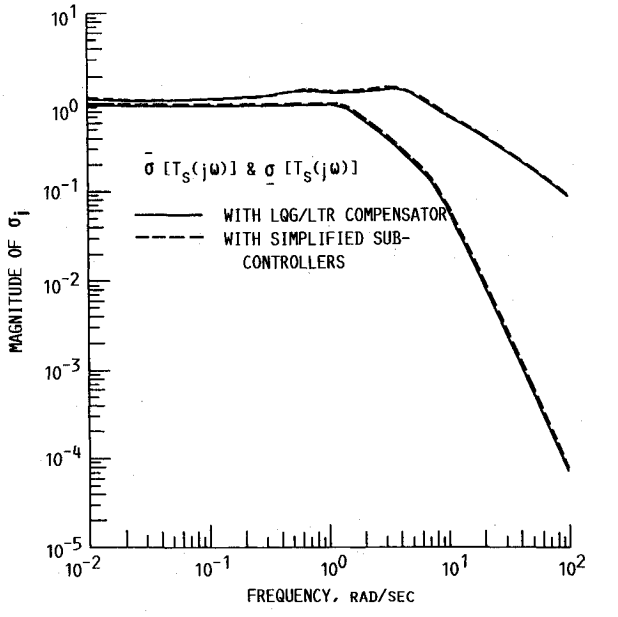

Fig. 7 Closed-loop system response comparison with LQG/LTR compensator and with partitioned, reduced, and simplified subcontrollers.

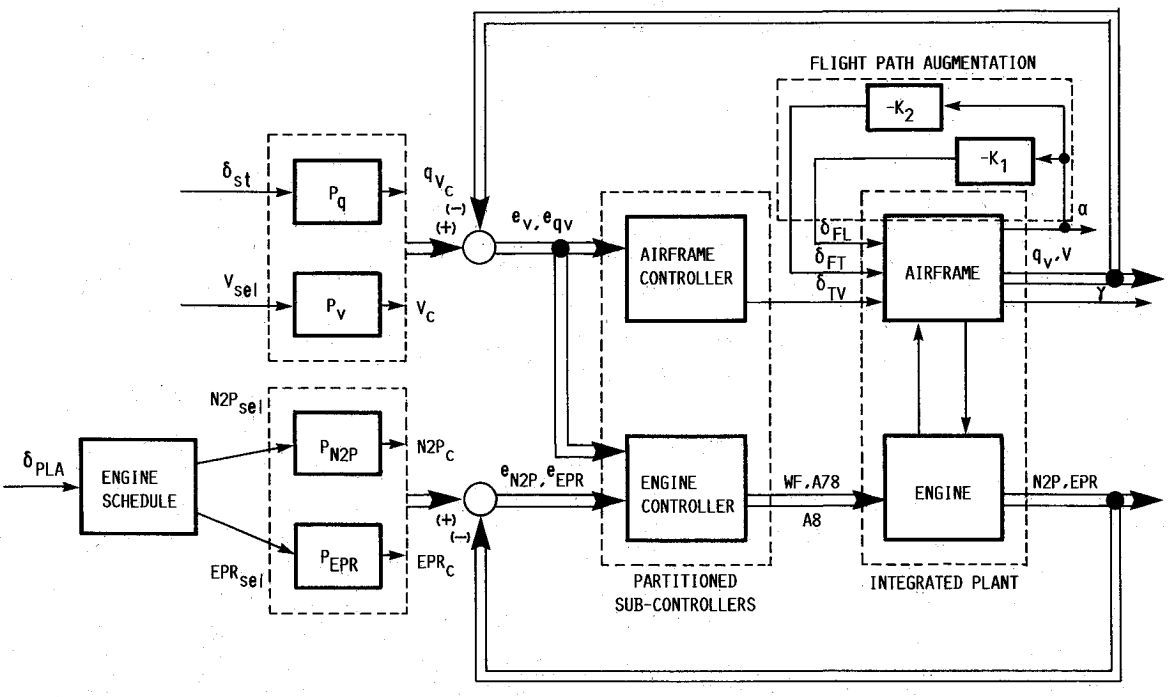

Fig. 8 Detailed implementation block diagram with simplified subcontrollers.

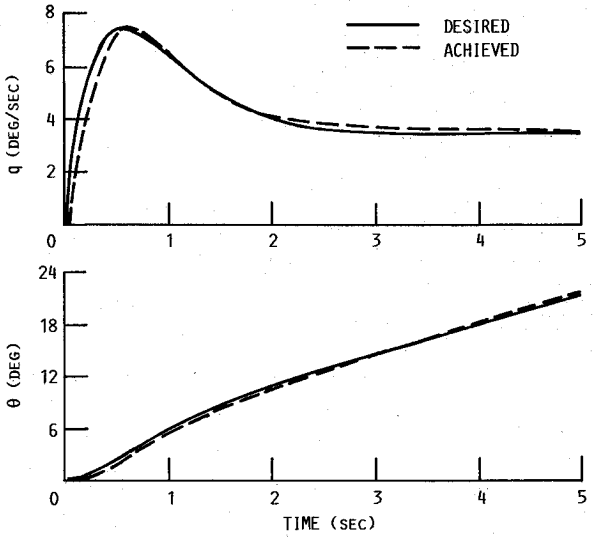

Fig. 9 Pitch rate q and attitude θ responses to step stick input ($\delta_{st} = 1$ in.).

The following steps were followed to obtain the command shaping prefilters that will give the desired response for each input/output pair:

1) The single-input/single-output system from the commanded variable to the response variable with all the feedback loops closed was first obtained ($y_i = T_i y_{c_i}$, where y_i is one of V, q_v, $N2P$, or EPR).

2) A reduced-order approximation (T_{r_i}) of T_i was obtained using internally balanced realization.

3) The procedure of Ref. 7 was applied to the reduced-order system T_{r_i} to obtain the command shaping prefilter P_i which will give the desired response.

4) The order of the prefilter was further reduced using the internally balanced realization approach.

The preceding process resulted in fourth-order prefilters for V, q_v, and $N2P$, and a first-order prefilter for EPR. The designed prefilters are listed in Table 2 in transfer function form. The desired and achieved pitch rate (q) and pitch attitude (θ) response to a unit step pilot stick input ($\delta_{st} = 1$ in.) are compared in Fig. 9. We note good agreement

Table 2 Design prefilter transfer functions

Notation: $\{K(1/\tau)[\zeta; \omega_n] = K(s + 1/\tau)(s^2 + 2\zeta\omega_n s + \omega_n^2)\}$

$$\frac{V_c}{V_{\text{sel}}} = \frac{0.013[0.67; 1.37](5.20)(830.21)}{[0.89; 0.31][0.56; 32.42]}$$

$$\frac{q_{v_c}}{\delta_{st}} = \frac{3.60(0.10)(0.51)(1.22)(5.61)}{(0)(0.67)[0.89; 2.24]}$$

$$\frac{N2P_c}{N2P_{\text{sel}}} = \frac{486.45[0.53; 4.05](66.93)}{(5.0)(13.03)[0.71; 90.50]}; \qquad \frac{\text{EPR}_c}{\text{EPR}_{\text{sel}}} = \frac{1.30(7.67)}{(10.0)}$$

between the desired and achieved pitch response. Time response comparisons for the other three variables of interest, as well as frequency-response Bode plot comparisons for all four variables, showed good agreement between the desired response and that achieved using the designed prefilters.

Finally, a comparison of the frequency-response Bode plots of pitch attitude and flight-path response to pilot stick input, θ/δ_{st} and γ/δ_{st}, respectively, showed that the flight-path to pitch attitude relationship in the region of the short period frequency can be approximated by a first-order lag with a time constant of 2 s. This is the reponse that was designed for by considering the angle of attack to flaps ($\alpha \to \delta_{FL}$ and $\alpha \to \delta_{FT}$) loop closures prior to the feedback compensator design.

Although these results indicate that the closed-loop system will meet the design specifications, it is important to check that the handling qualities parameters obtained using low-order equivalent system (LOES) approximation of the high-order closed-loop system satisfy the level I handling qualities requirements of the military specifications.[8] However, this could not be done for the present study because of time constraints.

Conclusions

Based on the example integrated flight/propulsion control system design presented in this paper, the following conclusions can be drawn regarding the strengths and weaknesses of the LQG/LTR-based integrated control design methodology:

1) The major drawback of the methodology is that it results in a single high-order integrated feedback compensa-

tor. Although such an integrated compensator is intuitively appealing in that it will lead to "optimum" performance, it may be unacceptable because of the difficulty of implementation as well as the desire to physically separate the flight and propulsion controllers.

2) The methodology is mainly geared toward synthesizing command tracking control laws; thus, one of its weaknesses lies in its inability to address the issue of plant augmentation. In this example study classical single-input/single-output control law design techniques had to be used to synthesize the desired flight-path augmentation prior to the application of the integrated control design methodology.

3) The singular value based robustness analysis tends to be highly conservative. Because of scaling (normalization) used in the control law synthesis procedure, the LQG/LTR procedure guarantees the stability robustness properties at a point in the loop that is internal to the compensator. Reducing the conservativeness of singular value stability robustness analysis and resolving the effect of scaling are issues that warrant further investigation.

The compensator partitioning approach, developed in this paper, led to much simplified subcontrollers without any significant loss in performance and stability robustness compared to that obtained with the full-order integrated compensator. The compensator partitioning approach needs to be validated for a system exhibiting higher degree of coupling between the subsystem dynamics than was the case in the present study.

Appendix

Vehicle system matrices:

$$A_p = \begin{bmatrix} -5.893e-02 & 1.067e-01 & -3.860e+01 & -3.184e+01 & 1.410e-02 & 3.144e-04 & 2.599e-04 & 3.819e-02 & 2.251e-03 \\ -2.659e-01 & -2.665e-01 & 1.948e+02 & -4.599e+00 & 5.196e-04 & -1.578e-05 & -2.106e-06 & 1.826e-04 & -2.957e-06 \\ -1.541e-03 & 7.806e-03 & -1.949e-01 & -4.818e-04 & 2.564e-05 & 9.463e-07 & 3.744e-07 & 3.668e-05 & 2.673e-06 \\ 0 & 0 & 1.0 & 0 & 0 & 0 & 0 & 0 & 0 \\ 1.427e-01 & -9.898e-01 & 0 & 2.006e+02 & 0 & 0 & 0 & 0 & 0 \\ 7.782e-01 & 1.542e-01 & 0 & 0 & -8.485e-02 & -4.191e+00 & 6.022e+00 & -3.434e+02 & 1.160e+01 \\ 1.518e-01 & 3.008e-02 & 0 & 0 & -1.655e-02 & 4.263e-01 & -5.707e+00 & 2.716e+01 & 1.040e+01 \\ 7.934e-01 & 1.572e-01 & 0 & 0 & -3.502e-01 & 2.295e-01 & 1.155e-01 & -9.024e+01 & 8.476e-01 \\ -1.005e-01 & -1.992e-02 & 0 & 0 & 1.096e-02 & 3.740e-02 & -1.036e-01 & -7.954e+00 & -1.068e+00 \end{bmatrix}$$

$$B_p = \begin{bmatrix} 3.468e-02 & -4.960e-02 & 3.436e-05 & -2.055e-01 & 6.912e-02 & -4.183e-04 \\ 6.925e-02 & -1.455e-01 & 1.234e-08 & -2.936e-04 & 7.104e-05 & -5.452e-01 \\ -8.100e-03 & 7.132e-04 & 5.507e-08 & 1.068e-04 & -8.383e-05 & -7.973e-02 \\ 0 & 0 & 0 & 0 & 0 & 0 \\ 0 & 0 & 0 & 0 & 0 & 0 \\ 0 & 0 & 1.469e-01 & 0 & 0 & 0 \\ 0 & 0 & 5.366e-02 & 0 & 0 & 0 \\ 0 & 0 & 1.813e-02 & -4.302e+01 & -2.583e+01 & 0 \\ 0 & 0 & 1.643e-01 & 0 & 0 & 0 \end{bmatrix}$$

$$C_\alpha = [-5.888e-02 \quad 2.796e-01 \quad 0 \quad 0 \quad 0 \quad 0 \quad 0 \quad 0 \quad 0]$$

$$C_p = \begin{bmatrix} 9.797e-01 & 1.941e-01 & 0 & 0 & 0 & 0 & 0 & 0 & 0 \\ 0 & 0 & 5.730e+01 & 5.730e+00 & 0 & 0 & 0 & 0 & 0 \\ 0 & 0 & 0 & 0 & 0 & 8.723e-03 & 0 & 0 & 0 \\ 0 & 0 & 0 & 0 & 0 & 0 & 0 & 6.803e-02 & 0 \end{bmatrix}$$

Scaling matrices:

$$S_u = \text{diag}[2.0e-04, \quad 0.02, \quad 0.01, \quad 0.1]$$

$$S_y = \text{diag}[0.05, \quad 0.3, \quad 0.2, \quad 3.0]$$

Reduced-order subcontroller matrices:

$$A_{c_a} = \begin{bmatrix} -5.873e+01 & -4.146e+01 \\ 4.146e+01 & -7.861e-02 \end{bmatrix}$$

$$B_{c_a} = \begin{bmatrix} -2.684e+01 \\ 9.322e-01 \end{bmatrix}$$

$$C_{c_a} = [2.684e+01 \quad 9.323e-01]$$

$$\Gamma_{ae} = \begin{bmatrix} 3.209e-01 & 2.491e-03 & -5.344e-03 \\ -1.482e-02 & 1.409e-03 & -5.143e-03 \end{bmatrix}$$

$$W_{ae} = [1.113e-04 \quad 6.345e-03 \quad -5.262e-03]$$

$$A_{c_e} = \begin{bmatrix} -1.671e-01 & -1.907e+01 & -1.526e-01 & 8.728e-04 & -1.040e+00 & 4.518e-01 & -2.837e-01 \\ 1.737e+01 & -2.023e+01 & -1.434e-01 & -1.579e-02 & -1.064e+01 & 1.036e+00 & 7.068e-02 \\ 9.982e-02 & -4.347e-02 & -1.213e+01 & 8.596e+00 & -1.698e-01 & 6.662e-03 & 9.724e-02 \\ -6.165e-03 & -9.159e-02 & -8.559e+00 & -1.856e-02 & -2.981e-02 & -4.037e-02 & 1.264e-03 \\ 1.170e+00 & -1.067e+01 & -2.406e-01 & -1.642e-02 & -1.928e+01 & -1.894e+01 & 2.991e+01 \\ 5.297e+00 & -1.411e+01 & -1.630e+00 & 1.159e-01 & -1.032e+02 & -3.599e+02 & 2.509e+02 \\ 8.426e-01 & -5.655e+00 & -3.689e-01 & -4.437e-03 & -3.562e+01 & -2.467e+02 & -2.091e+01 \end{bmatrix}$$

$$B_{ce} = \begin{bmatrix} -1.948e-02 & -1.872e-02 & 1.835e+00 \\ 2.746e-01 & 1.916e+01 & -7.368e-01 \\ -1.128e+01 & 2.138e-01 & -2.278e-01 \\ -3.723e-01 & 5.392e-02 & 2.792e-02 \\ 8.107e-02 & 5.754e+00 & -5.444e+00 \\ -6.793e-02 & 5.501e+00 & -2.934e+01 \\ -2.886e-02 & 2.508e+00 & -4.505e+00 \end{bmatrix}$$

$$\Gamma_{ea} = \begin{bmatrix} 2.858e-03 \\ -1.406e-02 \\ 9.420e-01 \\ 1.849e-01 \\ -8.075e-03 \\ -2.003e-02 \\ 4.307e-04 \end{bmatrix}$$

$$C_{ce} = \begin{bmatrix} 1.812e+00 & 1.914e+01 & 1.991e-01 & 2.549e-02 & 5.612e+00 & -1.449e+00 & 4.761e-01 \\ -1.366e-01 & 6.072e-01 & 8.751e+00 & -3.204e-01 & 3.561e+00 & 1.908e+01 & -3.284e+00 \\ -2.567e-01 & 1.056e+00 & -7.188e+00 & 2.705e-01 & 4.311e+00 & 2.292e+01 & -3.946e+00 \end{bmatrix}$$

$$W_{ea} = \begin{bmatrix} -2.408e-04 \\ -1.189e-02 \\ 9.894e-03 \end{bmatrix}$$

Subcontroller simplification:

$$\Gamma_{ae}(:,24:3) = 0; \qquad W_{ae} = 0; \qquad W_{ea} = 0$$

Acknowledgment

The authors thank Kevin Madden and P. D. Shaw, Flight Control Research Department, Northrop Corporation, Hawthorne, CA for providing the linearized aircraft models used in this study.

References

[1]Smith, K. L., "Design Methods for Integrated Control Systems," Wright-Patterson AFB, OH, AFWAL TR-86-2103, Dec. 1986.

[2]Shaw, P. D., Rock, S. M., and Fisk, W. S., "Design Methods for Integrated Control Systems," Aero Propulsion Laboratories, Wright-Patterson AFB, OH, AFWAL TR-88-2061, June 1988.

[3]Mihaloew, J., "Flight Propulsion Control Integration for V/STOL Aircraft," NASA TM-100226, Dec. 1987.

[4]Smith, K. L., Kerr, W. B., Hartmann, G. L., and Skira, C., "Aircraft Control Integration—Methodology and Performance Impact," AIAA Paper 85-1424, July 1985.

[5]Stein, G., and Athans, M., "The LQG-LTR Procedure for Multivariable Feedback Control Design," Massachusetts Inst. of Technology, Cambridge, MA, Rept. LIDS-R-1384, May 1984.

[6]Athans, M., "A Tutorial on the LQG/LTR Method," Massachusetts Inst. of Technology, Cambridge, MA, Rept. LIDS-P-1542, March 1986.

[7]Lehtomaki, N. A., Stein, G., and Wall, J. E., "Multivariable Prefilter Design for Command Shaping," AIAA Paper 84-1829, Aug. 1984.

[8]"Military Specification—Flying Qualities of Piloted Airplanes," USAF, Wright-Patterson AFB, OH, MIL-F-8785C, Nov. 1980.

[9]McRuer, D. T., Ashkenas, I., and Graham, D., *Aircraft Dynamics and Automatic Control*, Princeton Univ. Press, Princeton, NJ, 1973.

[10]Garg, S., "Model-Based Analysis and Cooperative Synthesis of Control and Display Augmentation for Piloted Flight Vehicles," PhD Dissertation, School of Aeronautics and Astronautics, Purdue Univ., West Lafayette, IN, May 1988.

[11]Garg, S., "Turbofan Engine Control System Design Using the LQG/LTR Methodology," NASA CR-182303, June 1989.

[12]Kwakernaak, H., and Sivan, R., *Linear Optimal Control Systems*, Wiley-Interscience, New York, 1972.

[13]Athans, M., Kapassouris, P., Kappos, E., and Spang, H. A., III. "Linear-Quadratic Gaussian with Loop-Transfer Recovery Methodology for the F-100 Engine," *Journal of Guidance, Control, and Dynamics*, Vol. 9, No. 1, 1986, pp. 45–52.

[14]Ridgley, B. D., Banda, S. S., McQuade, T. E., and Lynch, P. J., "Linear-Quadratic Gaussian with Loop-Transfer Recovery Methodology for an Unmanned Aircraft," *Journal of Guidance, Control, and Dynamics*, Vol. 10, No. 1, 1987, pp. 82–89.

[15]Lehtomaki, N. A., "Practical Robustness Measures in Multivariable Control System Analysis," PhD Dissertation, Massachusetts Inst. of Technology, Cambridge, MA, May 1981.

[16]Lehtomaki, N. A., Sandell, N. R., Jr., and Athans, M., "Robustness Results in LQG-Based Multivariable Control Design," *IEEE Transactions on Automatic Control*, Vol. AC-26, Feb. 1981, pp. 75–92.

[17]Garg, S., Mattern, D. L., and Bullard, R. E., "Integrated Flight/Propulsion Control System Design Based on a Centralized Approach," AIAA Paper 89-3520, Aug. 1989; also NASA TM-102137, July 1989.

[18]Ogata, K., *Modern Control Engineering*, Prentice-Hall, Englewood Cliffs, NJ, 1970.

[19]Safonov, M. G., and Doyle, J. C., *Minimizing Conservativeness of Robustness Singular Values*, edited by S. G. Tzefestas, Multivariable Control, Reidel, Dordrecht, the Netherlands, 1984, pp. 197–207.

[20]Apkarian, P. R., "Structured Stability Robustness Improvement by Eigenspace Assignment Techniques: A Hybrid Methodology," *Journal of Guidance, Control, and Dynamics*, Vol. 12, No. 2, 1989, pp. 162–168.

[21]Noble, B., and Daniel, J., *Applied Linear Algebra*, Prentice-Hall, Englewood Cliffs, NJ, 1977.

[22]Moore, B. C., "Principal Component Analysis in Linear Systems: Controlability, Observability, and Model Reduction," *IEEE Transactions on Automatic Control*, Vol. AC-26, Feb. 1981, pp. 17–31.

[23]Enns, D. F., "Model Reduction for Control System Design," PhD Dissertation, Dept. of Aeronautics and Astronautics, Stanford Univ., Stanford, CA, June 1984.